Synthesis, Characterization, and Structure Solution of CIT-5, a New, High-Silica, Extra-Large-Pore Molecular Sieve

Masahito Yoshikawa,[†,‡] Paul Wagner,[†] Mark Lovallo,[§] Katsuyuki Tsuji,[†] Takahiko Takewaki,[†] Cong-Yan Chen,[||] Larry W. Beck,[†] Chris Jones,[†] Michael Tsapatsis,[§] Stacey I. Zones,[||] and Mark E. Davis*[,†]

Division of Chemistry and Chemical Engineering, California Institute of Technology, Pasadena, California 91125, Department of Chemical Engineering, University of Massachusetts, Amherst, Massachusetts, 01003, and Chevron Research and Technology Co., Richmond, California

Received: May 7, 1998; In Final Form: June 23, 1998

The synthesis, structure solution, and characterization of the high-silica molecular sieve CIT-5 (California Institute of Technology Number 5) is described. CIT-5 is synthesized at hydrothermal conditions in the presence of *N*(16)-methylsparteinium and preferrably lithium cations. The structural solution of CIT-5 shows that it contains one-dimensional pores circumscribed by 14 tetrahedral atoms (14 MR). Rietveld refinement of the synchrotron X-ray powder data gives a symmetry and space group assignment for the structure of $Pmn2_1$ (no. 31) with refined unit cell parameters of $a = 13.6738(8)$ Å, $b = 5.0216(3)$ Å, and $c = 25.4883(7)$ Å ($V = 1750.1$ Å^3). Electron diffraction and transmission electron microscopy confirm the space group and the topology of the structure viewed along the [010] direction. Solid-state ^{29}Si NMR spectroscopy results are consistent with the space group assignment. The thermal/hydrothermal stability of CIT-5 compares well to that of other large- and extra-large-pore, high-silica molecular sieves. The acid form of CIT-5 is able to perform hydrocarbon reactions such as cracking and alkylation and shows behaviors that are different from other zeolites.

Introduction

Molecular sieves with 12 tetrahedral atoms (T-atoms) circumscribing the pores have been denoted as large-pore materials and have pore diameters of approximately 6−8 Å. Commercially useful zeolites such as NaY, L, and beta are large-pore materials. Pore systems that contain rings circumscribed by more than 12 T-atoms are classified as extra-large pores.[1] For many years, extra-large-pore materials have been aggressively pursued both in industry and in academia.[2−8] The demand for these materials is led by a desire to perform shape-selective adsorption and catalysis on molecules that are greater than 8 Å in size. Provided these extra-large-pore materials can retain their pore structures under the thermal or hydrothermal conditions required, they should find applications as catalysts in the petrochemical industry and show potential for use in the fine chemicals and pharmaceuticals industries as well.

The first extra-large-pore material, VPI-5[9] (an aluminophosphate material), was synthesized in 1987, and since that time numerous other phosphate-based extra-large-pore materials have been prepared.[3,10−14] These phosphate-based materials suffer from poor thermal and hydrothermal stability that limits their usefulness.

Recently, the high-silica molecular sieve UTD-1 has been characterized in detail and was shown to possess large, one-dimensional pores.[15,16] UTD-1 has the high thermal and hydrothermal stability characteristics of other high-silica molecular sieves and is the first high-silica molecular sieve to contain pores circumscribed by 14 tetrahedral atoms (14 MR). The synthesis of UTD-1 requires an organometallic structure-directing agent that can only be removed from the pores through calcination and acid treatment. Additionally, aluminum framework substitution (needed for acid catalysis) requires postsynthetic treatments.

Here, we report on the syntheses, characterization, and structural solution of CIT-5, a new, high-silica molecular sieve with 14-ring pores that is synthesized using an organic structure-directing agent. A preliminary report on the topology of CIT-5 has appeared, and here we provide the complete structure solution.[17] CIT-5 and UTD-1 are the only high-silica molecular sieves to contain these extra-large pores. The high thermal and hydrothermal stabilities of UTD-1 and CIT-5 confirm that extra-large-pore materials can have the stability required for industrial use. The direct incorporation of heteroatom substitutes such as aluminum into the framework of CIT-5 and the ease of removal of the structure-directing agent through calcination make this material an appealing catalyst for large molecules.

Experimental Section

Synthesis. CIT-5 was synthesized at hydrothermal conditions within a temperature range of 423−448 K. The syntheses were carried out in both sealed quartz tubes (75 × 15 mm i.d.) and Teflon-lined Parr reaction vessels. CIT-5 can be prepared from the following composition:

$$1\ SiO_2{:}0.1\ MOH{:}0.2\ MeSPAOH{:}x\ W{:}40\ H_2O$$

where W can include the following: $Ga(NO_3)_3$ (Aldrich), H_3-

* Address correspondence to this author at Division of Chemistry and Chemical Engineering, 210-41, California Institute of Technology, Pasadena, CA 91125 (818) 395-4251.
[†] California Institute of Technology.
[‡] Current address: Toray Industries Inc., Nagoya 455, Japan.
[§] University of Massachusetts.
[||] Chevron Research and Technology Co.

S1089-5647(98)02169-5 CCC: $15.00
Published on Web 08/21/1998

BO_3,(J. T. Baker), or $Al(NO_3)_3$ (J. T. Baker) (x can be varied from 0 to 0.02), and MOH can be either LiOH (Fisher) alone or a mixture of LiOH together with either NaOH (Aldrich) or KOH (Aldrich). As discussed below, CIT-5 can be formed in the absence of Li^+ cations if the alkali metal cation (K^+ or Na^+) is present in very low concentration ($[MOH]/[SiO_2]$ less than 0.05) when the total $[OH^-]/[SiO_2]$ ratio is held constant at 0.3. The synthesis of the organic structure-directing agent, *N*(16)-methylsparteinium hydroxide (**I**) (MeSPAOH), has been previ-

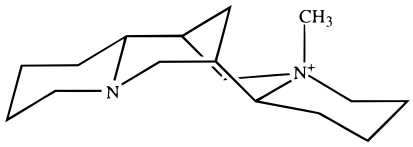

I

ously described.[18]

In a typical synthesis preparation of pure-silica CIT-5, 0.019 g of LiOH is added to a solution of 4.21 g of distilled, deionized water and 0.85 g of a 50.0 wt % solution of N(16) methylsparteinium hydroxide. Then, 1.60 g of the colloidal silica source (HS-30 DuPont) is added, and the mixture is stirred for 30 min. The resulting synthesis mixture is charged into quartz tubes that are heat sealed and placed in a convection oven at 175 °C for 3−7 days. The recovered solid is washed with distilled, deionized water and allowed to air-dry.

Analytical. *X-ray Diffraction.* Synchrotron powder X-ray diffraction (SPXRD) patterns were collected on the X7A synchrotron beam line at Brookhaven National Laboratory. The CIT-5 sample was prepared for data collection by first calcining the material at 923 K (heating from room temperature at 5 K/min). The calcined sample was then packed into a 1-mm glass capillary, and the synchrotron data were collected at ambient conditions with a step size of 0.005° from 4° to 50° 2-θ at a wavelength of 1.147 98 Å. Powder X-ray diffraction patterns were also obtained on a Scintag XDS 2000 diffractometer using CuKα radiation (λ = 1.541 84 Å) with a liquid-nitrogen-cooled solid-state germanium detector in a Bragg−Brentano configuration. The diffraction data were collected in continuous scanning mode over the range 2° < 2-θ < 51° with a scanning rate of 0.2°/s. National Institute of Standards and Technology Standard Reference Material 675 (fluoropholog opite mica) was used as the external standard.

The thermal and hydrothermal stability of CIT-5 were studied by in situ, temperature-programmed powder X-ray diffraction. The samples were mounted as thin films on a platinum−rhodium alloy heater filament inside an Edmund Buhler high-temperature X-ray diffraction chamber. The sample thickness of the calcined CIT-5 powder on the filament varied from 0.5 to 1 mm. The chamber was evacuated and refilled with the flow gas, and a steady flow of 0.5 L/min was then maintained during data collection. The flow gas for the thermal stability studies was dry nitrogen, while dry nitrogen bubbled through distilled water held at room temperature was used as the flow gas for the hydrothermal stability studies. The samples were heated at a rate of 10 K/min and held at the designated temperature for 15 min prior to data collection. The X-ray diffraction scans were collected as continuous scans from 2° to 51° 2-θ at a scan rate of 5°/min.

Physisorption Studies. Argon physisorption measurements were carried out on a Coulter Omnisorp 100CX adsorption instrument. Argon adsorption isotherms were measured at 87 K by both static and continuous-flow techniques. Prior to the adsorption experiments, the calcined samples were degassed under vacuum ($<10^{-6}$ Torr) at 573 K for 2 h. Approximately 1000 data points were obtained from the continuous flow experiments with argon pressures ranging between 10^{-6} and 550 Torr. Sample sizes were ∼100 mg, and the argon flow rate was low enough to require 1−2 h to admit enough argon to fill the sample micropores. The equilibration times for the static adsorption experiments were 10 min for each data point. Doses were small enough so that 5−10 h were required to admit enough argon to fill the micropores. Micropore volumes and external areas were estimated from α-plot analyses of the adsorption isotherms, using α values obtained from a silica standard (CPG-75). The adsorption capacities of zeolites for vapor-phase hydrocarbons were measured at room temperature using a Cahn C-2000 balance coupled with a computer via an ATI−Cahn digital interface. The adsorbates studied were *n*-hexane, 2,2-dimethylbutane, cyclohexane, and 1,3,5-triisopropylbenzene. The vapor of the adsorbate was delivered from the liquid phase. The relative vapor pressure P/P_0 was maintained at ∼0.3 by controlling the temperature of the liquid adsorbate using a cooling circulator. Prior to the adsorption experiments, the calcined zeolites were dehydrated at 623 K under a vacuum of 10^{-3} Torr for 5 h. The adsorption capacities are reported in milliliters of liquid per gram of dry zeolite, assuming bulk liquid density for the adsorbate in the micropores.

Catalytic Studies. Three catalytic test reactions are reported using the acid form of CIT-5: cracking of C6 isomers, *m*-xylene isomerization, and hydrocracking of *n*-hexadecane. The CIT-5 material was synthesized as previously described, with the exception that highly dealuminated Y zeolite (TOSOH HUA 390) was used as the silica source.[19] The syntheses were carried out in Teflon-lined Parr reactors heated to 433 K while rotating, for a period of 6−10 days.

The active CIT-5 catalyst was prepared by calcining the as-synthesized CIT-5 to 873 K in air, followed by ion exchange of the calcined material with ammonium nitrate. The ion exchange was carried out by heating 1 g of the calcined zeolite with 1 g of ammonium nitrate in 50 mL of water at 363 K for 2 h, followed by filtration, washing with water, and finally air-drying. The ammonium-exchanged zeolite was then packed into the catalytic reactor and converted to the acid form by heating to 813 K in situ. The acid form of CIT-5 was used for the cracking of C6 isomers and for the isomerization of *m*-xylene. The test reaction involving the hydrocracking of *n*-hexadecane (a model compound) utilized an acid/palladium form of the zeolite (as described below).

The cracking of C6 isomers was carried out as follows: 500 mg of ammonium-exchanged CIT-5 (20−40 mesh after pelleting at 3 kpsi and breaking the pellet) was calcined to 813 K for 4 h and cooled under a flow of nitrogen. The catalyst was then placed in a 3/8 in. stainless steel reactor with a bed of alundum packed on either side of the catalyst. Helium was passed through the reactor at 10 cm^3/min while the reactor tube was heated by a Lindburg furnace. At a reactor tube temperature of 645 K, a 50/50 (w/w) feed of *n*-hexane and 3-methylpentane was introduced by a downflow (controlled using a Brownlee pump) of 8 μL/min. On-line sampling via a Valco 6-way valve was started after 10 min of feed delivery. The data were collected on a Hewlett-Packard 5880 gas chromatograph with product peaks assigned using standards.

The *m*-xylene isomerization test reactions were conducted using two CIT-5 samples as catalysts. Sample A had a silica-to-alumina ratio (SAR) of 200, and sample B a silica-to-galia ratio (SGR) of 100. Sample A was syntheszied using a dealuminated Y zeolite as the silicon source, while sample B

TABLE 1: Synthesis of CIT-5[a]

SiO_2	MOH	MeSPAOH	W	H_20	temp (°C)	time (days)	phase (silicon/Y)[b]
1	0.1 LiOH	0.2		40	175	5	CIT-5
1	0.05 KOH	0.25		40	175	60	CIT-5 + AFI
1	0.05 NaOH	0.25		40	175	18	CIT-5
1	0.1 NaOH	0.2		40	175	7	AFI
1	0.075 LiOH, 0.025 NaOH	0.2	0.01 H_3BO_3	40	175	5	CIT-5
1	0.050 LiOH, 0.050 NaOH	0.2	0.01 H_3BO_3	40	175	5	AFI
1	0.075 LiOH, 0.025 KOH	0.2	0.01 H_3BO_3	40	175	5	CIT-5
1	0.1 LiOH	0.2	0.01 H_3BO_3	40	175	7	CIT-5 (63)
1	0.1 LiOH	0.2	0.01 $Al(NO_3)_3$	40	175	11	CIT-5 (95)
1	0.1 LiOH	0.2	0.01 $Ga(NO_3)_3$	40	175	7	CIT-5 (109)

[a] Values for reactants in table are given as mole ratios. [b] Values in parentheses are the molar Si/Y ratios (Y: Ga, Al, or B) measured by elemental analysis.

was synthesized using colloidal silica as the silicon source. After conversion of the CIT-5 material to the acid form (mesh size 35−70), 100−400 mg of the catalyst was added to a downflow reactor. Under a helium flow of 50 mL/min, the following temperature program was carried out: the reactor was heated to 448 K over 2 h and held at this temperature for an additional 2 h, the temperature was then increased from 448 to 623 K over 1.5 h and held at 623 K for 3 h, and finally, the temperature of the reactor was reduced to 590 K over 25 min. Once the helium flow rate had been reduced to 20 mL/min, the feed was introduced by passing the helium flow gas through a saturator with *m*-xylene at 283 K. The products were analyzed on-line as previously described.

The catalyst used in the hydrocracking experiments was prepared by ion-exchange of the palladium cations into the ammonium-exchanged material. Palladium tetraamine dinitrate was dissolved in a solution containing 2 mL of 0.156 N NH_4-OH in 9 mL of H_2O (the quantity of palladium tetraamine dinitrate dissolved was such that if all the palladium were to exchange into the zeolite there would be 0.5 wt % Pd in the catalyst). Next, 990 mg of the zeolite was introduced into the solution, which was then aged statically at room temperature for 3 days. The zeolite was filtered, washed with 200−300 mL of water, and then calcined to 755 K in air using the following program: the catalyst was heated to 393 K and held at this temperature for 2 h and the temperature was then ramped to 755 K at 1 K/min and held at 755 K for 3 h. The material was then pelleted, broken and meshed to 20−40, and jacketed by quartz chips of the same mesh size. The packed zeolite catalyst was dried in situ, and the reactor temperature was reduced to 588 K. The inert carrier gas was replaced with a hydrogen atmosphere at 1200 psi. The *n*-hexadecane was introduced at a flow rate of 1 μL/min. The temperature of the catalyst was gradually increased to promote a higher conversion of the feed. After 167 h on-stream at 622 K, a 96% conversion of *n*-hexadecane to isomers and lighter products was achieved.

NMR Studies. Solid-state NMR spectra were collected on a Bruker AM 300 spectrometer. Samples were packed into 7 or 4 mm ZrO_2 rotors and spun in air. ^{29}Si NMR spectra (59.63 MHz) were obtained using magic angle spinning (MAS) at spinning rates of 3−4 kHz, pulse widths of 6 ms, and recycle delays of 30−60 s. Tetrakis(trimethylsilyl)silane was used as the external reference material for ^{29}Si and ^{13}C NMR chemical shift determination. All chemical shifts are reported in ppm relative to TMS. ^{27}Al NMR spectra were recorded at a frequency of 78.2 MHz on samples packed into a 4-mm ZrO_2 rotor spinning at 8−9 kHz. A pulse width of 4 ms corresponding to a flip angle of $\pi/2$ along with a recycle delay of 1 s were used. ^{27}Al NMR chemical shifts are referenced to a 1.0 M $Al(NO_3)_3$ solution (= 0.00 ppm) and are not corrected for second-order quadrupolar effects. ^{13}C NMR spectra (75.45 MHz) were measured using cross-polarization with a 1 H-90° pulse of 6.5 ms with a recycle delay of 1 s. ^{13}C NMR chemical shifts are referenced to adamantane (downfield resonance at 38.4 relative to TMS). Spectral deconvolution and simulation were performed using both the Bruker Linesim and the MacFID software packages.

TEM Studies. Samples for transmission electron microscopy (TEM) were prepared both by microtomy and by dispersion. The samples prepared by dispersion were first crushed and then sonicated in ethanol. A drop of this dispersion was transferred to a carbon-coated Cu grid and allowed to dry. The samples prepared by microtomy were embedded in an epoxy (LR White) which was subsequently cured at 363 K for 2 h. Slices from the hardened epoxy sample were prepared using a diamond knife mounted on an ultra-microtome. The samples were dried in a desiccator overnight prior to mounting in the TEM specimen holder. The TEM, ED, and HREM images were taken on a JEOL 2000 FX operating at 200 kV, a JEOL 100CX operating at 100 kV, and a Phillips 430 operating at 200 kV, respectively. Image analysis was performed using the "Image" software for Macintosh.

Additional Characterization Studies. Scanning electron micrographs were collected on a Camscan Series 2-LV electron microscope operating at an acceleration voltage of 15 kV. A DuPont 951 thermogravimetric analyzer was used to carry out the thermogravimetric analysis using a constant heating rate of 5 K/min. The elemental analyses were performed by Galbraith Laboratories (Knoxville, TN).

Results and Discussion

Synthesis. Pure-silica CIT-5 is formed from the following synthesis mixture (mole ratio):

$$1\ SiO_2{:}0.1\ LiOH{:}0.2\ MeSPAOH{:}40\ H_2O$$

at a temperature of 448 K upon heating for 5 days. The optimal synthesis conditions include Li^+ cations ([LiOH]/[SiO_2] = 0.1); however, ratios of Li^+/M^+ (where M^+ can be either Na^+ or K^+) as low as 3/1 do not hinder the formation of CIT-5 (Table 1). As the Li^+/M^+ ratio is decreased to 1/1, CIT-5 is not formed and the synthesis results in the production of a previously reported, high-silica phase, SSZ-24[18,20,21] (International Zeolite Association code: AFI).[22] CIT-5 can be formed without Li^+ present in the synthesis mixture at much longer crystallization times (>20 days), provided an alkali cation (K^+ or Na^+) is present in low concentrations ([MOH]/[SiO_2] ratios less than 0.05) and the ratio of [OH^-]/ [SiO_2] is held constant at 0.3 (synthesis results are summarized in Table 1). As the concentration of Na^+ is increased at constant [OH^-] ([NaOH]/[SiO_2]

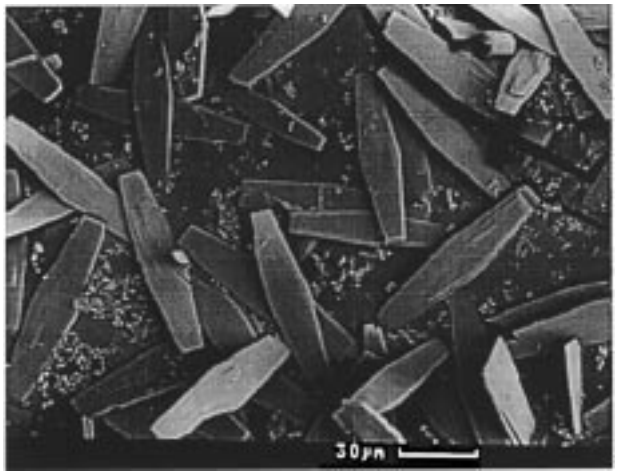

Figure 1. Scanning electron micrograph of CIT-5 crystallites.

ratio is increased from 0.05 to 0.1), SSZ-24 is formed to the exclusion of CIT-5.

These synthesis results indicate that the organic methylsparteinium cation weakly structure-directs CIT-5. The presence of Li^+ cations serves to accelerate the crystallization times, while the presence of other alkali metal cations (Na^+ or K^+) at low concentrations also weakly assists in the crystallization of CIT-5. At higher concentrations, the presence of the Na^+ cations dominates the structure direction toward SSZ-24, presumably by affecting the silica dissolution kinetics or stabilizing species in solution prior to nucleation, leading to the stabilization of SSZ-24 growth units. The organic methylsparteinium cations may then serve to further stabilize the forming SSZ-24 structure by filling the pore system.

CIT-5 has also been synthesized in the presence of various atoms that can substitute for silicon, e.g., gallium, boron, and aluminum. The elemental analyses results for the aluminum-containing CIT-5 (Al-CIT-5) indicate a silicon-to-aluminum ratio of 95. The chemical shift of the ^{27}Al resonance in the ^{27}Al MAS NMR spectrum from the as-synthesized Al-CIT-5 and the catalytic data for the Al-CIT-5 material both confirm the presence of tetrahedrally coordinated aluminum and the Bronsted acid site formed from the framework aluminum (both results will be discussed in greater detail below).

Scanning electron micrographs (SEMs) show the CIT-5 crystallites to have a thin flat plate morphology (Figure 1). TEM/ED analysis of the flat plate crystals reveal the (301) lattice fringes (Figure 2) running along the long axis of the crystals and indicates that the *b*-axis (parallel to the channel direction) coincides with the long axis of the crystals.

Structure Solution of CIT-5. Synchrotron powder X-ray data (SPXRD) were collected from a sample of the calcined pure-silica CIT-5. Indexation of the SPXRD revealed an orthorhombic crystal class for the pure-silica CIT-5 sample with refined unit cell parameters of $a = 13.6738(8)$ Å, $b = 5.0216(3)$ Å, and $c = 25.4883(7)$ Å ($V = 1750.1$ Å^3).[23] Initial analysis of the systematic absences in the SPXRD data indicate body centering consistent with six possible space groups.

The starting model for Rietveld refinement[24] was obtained by an iterative process of model building, distance least squares (DLS)[25] refinement of the atomic positions for the model, and comparison of the simulated powder X-ray pattern (CERIUS)[26] to the experimental pattern. The model with the closest match between the simulated X-ray powder pattern and the experimental XRD was found to have maximal topological symmetry of space group *Imma* (no. 74, standard setting), consistent with the systematic absences. However, initial Rietveld refinement of the starting model in this space group indicated an unacceptably large variation in the Si−O bond distances and the O−Si−O bond angles.[17]

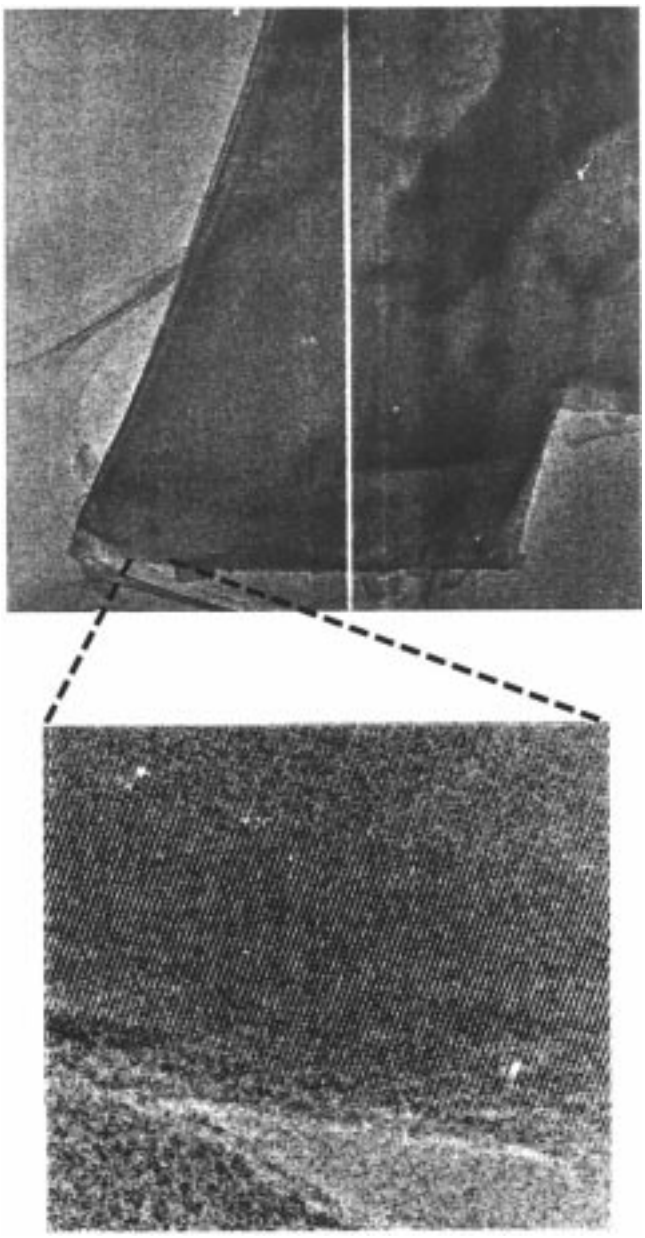

Figure 2. Transmission electron micrograph of pure-silica CIT-5 crystallite showing (301) lattice fringes indicting pore direction parallel to the long axis of the crystallite.

To obtain a reasonable refinement of the SPXRD data, it was necessary to reduce the topological symmetry of the space group within the orthorhombic crystal class. Distance least squares (DLS) refinement was used as a guide for indicating reasonable structural parameters for the starting model in a given space group. The DLS residual values for the six orthorhombic subgroups of *Imma* (*Imm*2, $I2_12_12_1$, *Pmma*, *Pnma*, *Pnna*, and *Pmna*) are summarized in Table 2. Although the space group *Pmna* gives the lowest DLS *R* value (0.0050), it is high in comparison to other high-silica zeolite and indicates distortions in the structural parameters. As a result, the four orthorhombic subgroups of *Pmna* were also evaluated using DLS as a guide. Of these subgroups, space group $Pmn2_1$ was found to give the lowest *R* value (0.0032).

TABLE 2: CIT-5 Space Group Analysis

space group	DLS *R*-value[a]	preliminary Rietveld refinement wR$_p$	R_p	reduced χ^2
Imma	0.0171			
orthorhombic subgroups of *Imma*				
*Imm*2	0.0150			
$I2_12_12_1$	0.0088			
Pmma	0.0153			
Pnma	0.0096			
Pnna	0.0076			
Pmna	0.0050	0.1107	0.0853	91.23
orthorhombic subgroups of *Pmna*				
*Pnc*2	0.0047	0.1040	0.0771	80.08
$P222_1$	0.0049	0.1186	0.0859	102.90
*Pma*2	0.0036	0.1051	0.0784	80.95
$Pmn2_1$	0.0032	0.1028	0.0762	77.33

[a] DLS refinements carried out using the following orthorhombic unit cell parameters (Å): 5.021, 13.697, 25.497.

Initial Rietveld refinements were carried out in the space group *Pmna* and in each of its four orthorhombic subgroups (*Pnc*2, $P222_1$, *Pma*2, and $Pmn2_1$). The atomic coordinates obtained from the DLS refinements were input as starting models for the Rietveld refinements. The initial Rietveld refinement procedures were carried out similarly for each of the space groups, and the results are summarized in Table 2. Examination of the DLS *R* values and the initial Rietveld wR$_p$, R_p and reduced χ^2 values led to the selection of space group $Pmn2_1$ for further refinements of the CIT-5 starting model.

The initial atomic positions for the Rietveld refinement of CIT-5 in space group $Pmn2_1$ (no. 31, standard setting) were obtained from the DLS refinement. During the initial stages of the refinement, the scale factor and zero shift were refined along with a 15-parameter shifted Chebyshev function[24] for background subtraction. The lattice parameters and the peak shape function parameters[27] were then refined until convergence of the *R* values was obtained. Soft geometric constraints for the Si−O bond distances (d(Si−O) = 1.610(10) Å) and interatomic O−O distances (d(O−O) = 2.610(10) Å) were employed for the initial stages of the atomic position refinement. The weighting factor for the soft geometric constraints was gradually reduced. However, complete elimination of the soft constraints caused slight distortions in the Si−O bond distances and O−Si−O angles.

Table 3 provides a summary of the refinement details. All structural parameters are within reasonable ranges for silicate materials.[28] The average bond distance, d(Si−O), is 1.591 Å with a range of 1.555−1.641 Å. The average Si−O−Si angle is 149.4° with a maximum of 168.7° and a minimum of 140.6°, and the average O−Si−O angle is 109.4° with a maximum value of 113.8° and a minimum value of 104.2°. The low Rietveld residuals values (wR$_p$ = 7.09%, R_p = 5.40%) indicate a close fit between the calculated and the experimental pattern (Figure 3). This solution has been accepted by the International Zeolite Association Structure Commision and the code CFI has been established for CIT-5.

The structure of CIT-5 viewed down the *b*-axis (Figure 4) is composed of one-dimensional, extra-large pores of nearly circular cross section (center of oxygen to center of oxygen distance 9.91 × 9.87 Å^2) circumscribed by 14 T-atoms. The asymmetric unit contains 10 T-atoms and 19 oxygen atoms, resulting in a unit cell content of [$Si_{32}O_{64}$], a framework density of 18.3 T-atoms/1000 Å^3, and a density of 1.821 g/cm^3. Table 4 contains the final atomic positional parameters obtained from the Rietveld refinement.

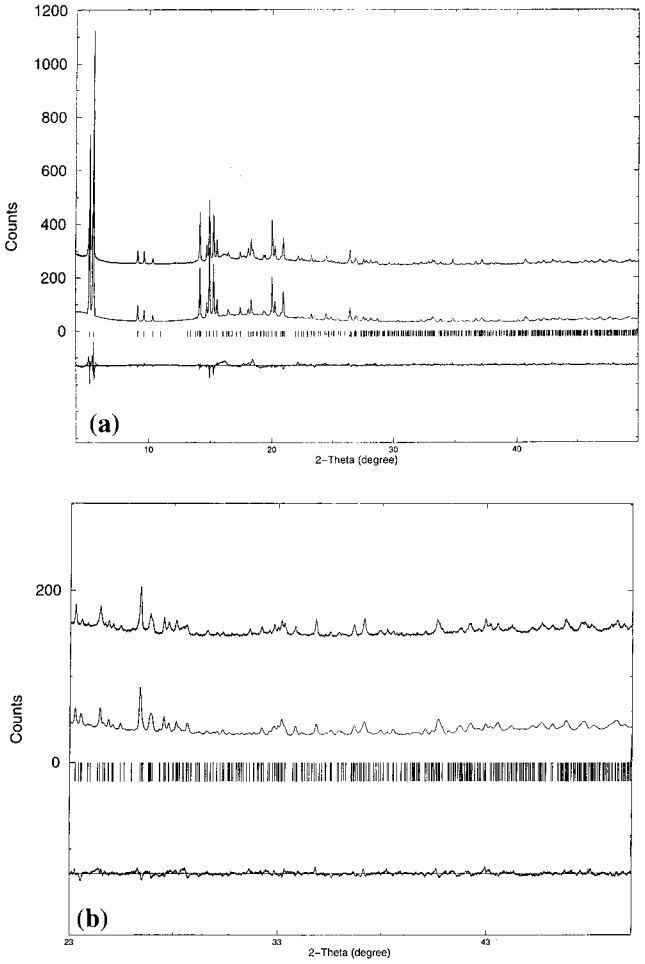

Figure 3. Comparison of experimental synchrotron pattern (upper) calculated (middle) and difference profile (lower) for the Rietveld refinement of CIT-5 (λ = 1.147 98 Å).

TABLE 3: Crystallographic and Refinement Data

space group	$Pmn2_1$ (no. 31)
a	13.67388(40) Å
b	5.02163(12) Å
c	25.48837(95) Å
wavelength	1.14798 Å
data collection temp	298 K
profile range	4.0−50.0°
no. of observables	9200
step scan increments	0.005°
no. of variables	131
no. of reflections	449
wR$_p$	7.09%
R_p	5.40%
av d(Si−O)	1.591(3) Å
min	1.555(0) Å
max	1.641(0) Å
av Si−O−Si angle	149.4(5)°
min	140.6(0)°
max	168.7(0)°
av O−Si−O angle	109.4(5)°
min	104.2(0)°
max	113.8(0)

TEM/ED Studies. The simulated, experimental, and image-processed experimental high-resolution transmission electron micrographs (HRTEM) of CIT-5 viewed down the 14-MR pores are shown in Figure 5. Comparison of the experimental image to the simulated image confirms the proposed topology. The CIT-5 topology consists of zigzag ladders of 4-rings with pendant 5-rings. These units are interconnected through single zigzag chains to produce the pseudo-body-centered structure.

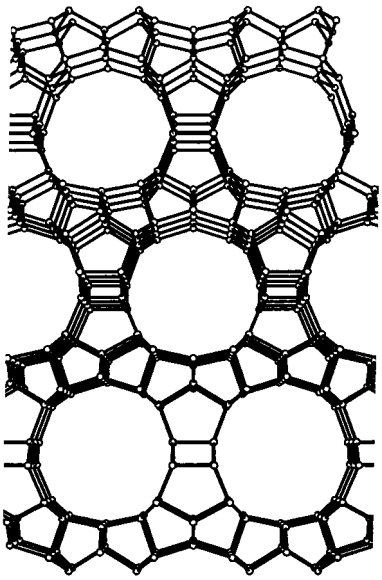

Figure 4. CIT-5 framework structure (bridging oxygen atoms omitted) viewed down 14 MR pores ([010] zone).

TABLE 4: Refined Atomic Positional Parameters (Fractional Coordinates) in Space Group *Pmn*2$_1$ (no. 31) and Isothermal Temperature Factors (Esd in Parentheses)

atom	*x*	*y*	*z*	U_{iso}(Å^2)
Si1	0.1100(10)	0.2980(4)	0.0318(6)	0.019(1)
Si2	0.000000(0)	0.7300(5)	0.2702(7)	0.048(9)
Si3	0.2868(9)	0.733(33)	0.1883(5)	0.010(3)
Si4	0.000000(0)	0.2360(4)	0.2055(6)	0.041(2)
Si5	0.1956(20)	0.250(4)	0.1414(5)	0.017(2)
Si6	0.3884(9)	0.2082(34)	0.4634(5)	0.027(5)
Si7	0.3001(12)	0.300(4)	0.3523(6)	0.034(8)
Si8	0.500000(0)	0.764(4)	0.2248(5)	0.016(7)
Si9	0.500000(0)	0.264(5)	0.2912(7)	0.009(6)
Si10	0.2064(12)	0.789(4)	0.3076(6)	0.038(8)
O11	0.1258(22)	0.091(32)	−0.0139(6)	0.027(8)
O12	0.1834(7)	0.242(4)	0.0794(33)	−0.025(6)
O13	0.1391(20)	0.5933(32)	0.0092(7)	0.013(5)
O14	0.000000(0)	0.303(9)	0.0518(10)	0.041(9)
O15	0.000000(0)	0.425(4)	0.2541(7)	0.039(5)
O16	0.0926(6)	0.782(4)	0.3075(7)	0.049(7)
O17	0.000000(0)	−0.071(4)	0.2216(7)	0.005(5)
O18	0.2742(13)	0.465(5)	0.1581(8)	0.029(2)
O19	0.4029(5)	0.796(4)	0.1906(6)	0.003(5)
O20	0.2337(14)	−0.036(4)	0.1584(8)	0.008(4)
O21	0.2433(16)	0.728(5)	0.2476(5)	0.023(6)
O22	0.9053(6)	0.3024(34)	0.1694(5)	0.006(6)
O23	0.3164(13)	0.238(5)	0.4141(5)	0.065(5)
O24	0.500000(0)	0.241(8)	0.4453(10)	0.017(9)
O25	0.2333(14)	0.083(4)	0.3260(8)	0.037(2)
O26	0.4043(6)	0.303(5)	0.3256(6)	0.044(0)
O27	0.2529(15)	0.584(4)	0.3468(7)	0.039(3)
O28	0.500000(0)	−0.037(5)	0.2716(8)	0.057(7)
O29	0.500000(0)	0.464(4)	0.2446(8)	0.003(1)

Electron diffraction patterns from the principal axes (Figure 6) of pure-silica CIT-5 crystals contain considerable dynamical diffraction effects. However, they show no signs of streaking, indicating that the crystals are neither faulted nor disordered.

NMR Studies. Comparison of the liquid ^{13}C NMR of N(16)-methylsparteinium hydroxide with the MAS ^{13}C NMR of the as-synthesized CIT-5 (shown in Figure 7) indicates that the structure-directing agent occluded in the pores of CIT-5 is intact and has not decomposed under the synthesis conditions. The ^{29}Si MAS NMR spectrum of the as-made and calcined CIT-5 are shown in Figures 8a and 8b. The ^{29}Si NMR resonances from −107 to −115 ppm lie within the typical Q^4 range reported for other high-silica zeolites.[29] The NMR spectra of the calcined

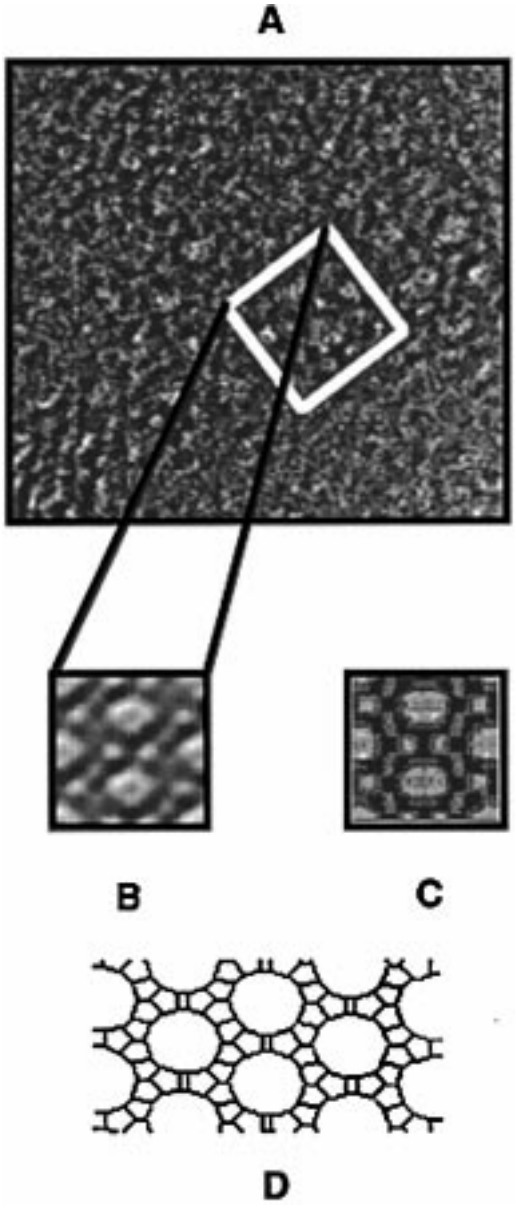

Figure 5. Transmission electron micrographs (TEMs) of CIT-5: (a) experimental image, (b) experimental averaged image, (c) simulated TEM image of CIT-5 topology, and (d) CIT-5 topology.

material has been deconvoluted into five peaks: −107.8 (11.4%), −108.3 (25.7%), −112.9 (26.7%), −113.2 (25.9%), and −114.9 (10.3%) (Figure 8c).

The basis set for the CIT-5 model in space group *Pmn*2$_1$ contains 10 T-atoms. However, half of the T-atoms in the asymmetric unit are related by a pseudo-2-fold symmetry operation at (1/4,1/4,z) that exists in the highest maximal topology. The similarities in the chemical environments of these T-atoms and the resolution limitations in the NMR intrumentation reasonably account for the observed deconvolution of the ^{29}Si MAS NMR of the calcined Si-CIT-5 sample. The site populations for the CIT-5 model in space group *Pmn*2$_1$ [Si2 + Si8 (4), Si1 + Si6 (8), Si3 + Si10 (8), Si5 + Si7 (8), Si4 + Si9 (4)] corresponds to a relative intensity ratio of 1:2:2:2:1 consistent with the observed deconvolution.

The ^{27}Al MAS NMR spectrum of the as-synthesized Al-CIT-5 shows a single peak at 54 ppm. This peak is assigned to tetrahedrally coordinated aluminum and is a strong indication that the aluminum present in the material has been incorporated into the framework.

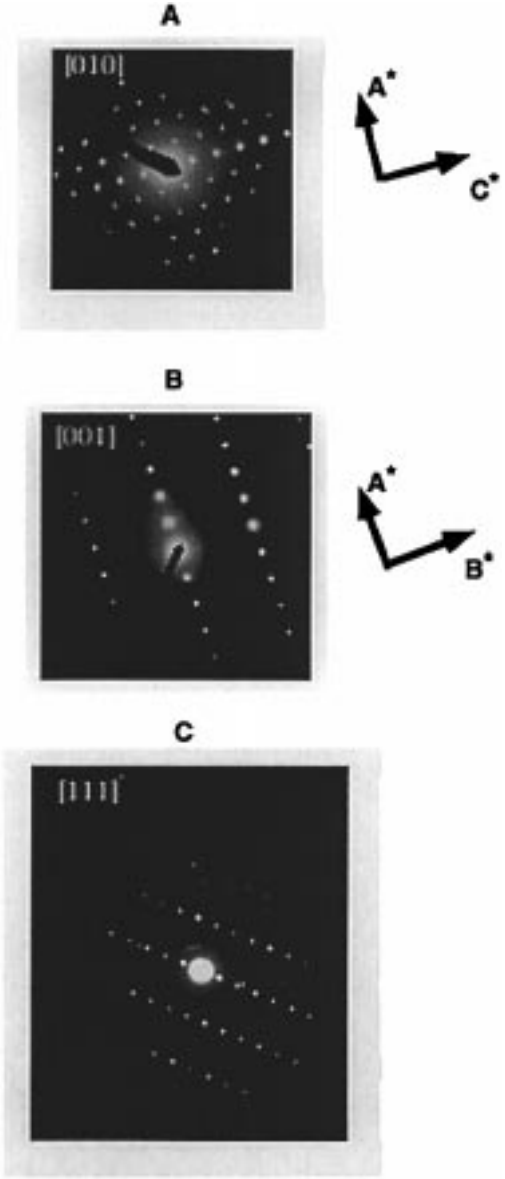

Figure 6. Electron diffraction patterns from pure-silica CIT-5: (a) [010], (b) [001], and (c) [111]. The reciprocal lattice vectors are shown for the principal zone axes [010] and [001].

Adsorption and Thermal Gravimetric Studies. The adsorption capacities of various organic molecules in CIT-5 are reported in Table 5. The adsorption capacity of 1,3,5-triisopropylbenzene is consistent with the presence of extra-large, one-dimensional pores in CIT-5. The adsorption capacities of the other organic molecules listed in Table 5 for CIT-5 are similar to those reported for other large- and extra-large-pore zeolites, e.g., UTD-1[16] and SSZ-24.[19,20] While the pore-mouth openings of CIT-5 and SSZ-24 are similar, the CIT-5 topology contains side pockets within the pore system (parallel to the *c* direction) that results in a maximum free pore diameter of 10.72 Å and explains the differences in the uptake of large organic molecules such as 1,3,5-triisopropylbenzene (~8.5 Å kinetic diamter). The calculated geometric void volume for CIT-5 is 0.13 mL/g and compares well to the argon physisorption results reporting 0.11 mL/g. In addition, the thermal gravimetric analysis shows an 11.2 wt % loss from the SDA, N(16)-methylsparteinium. This amount of organic corresponds to 1 SDA molecule per unit cell, resulting in a pore volume of 0.13 mL/g, consistent with the argon physisorption and the calculated geometric void volume.

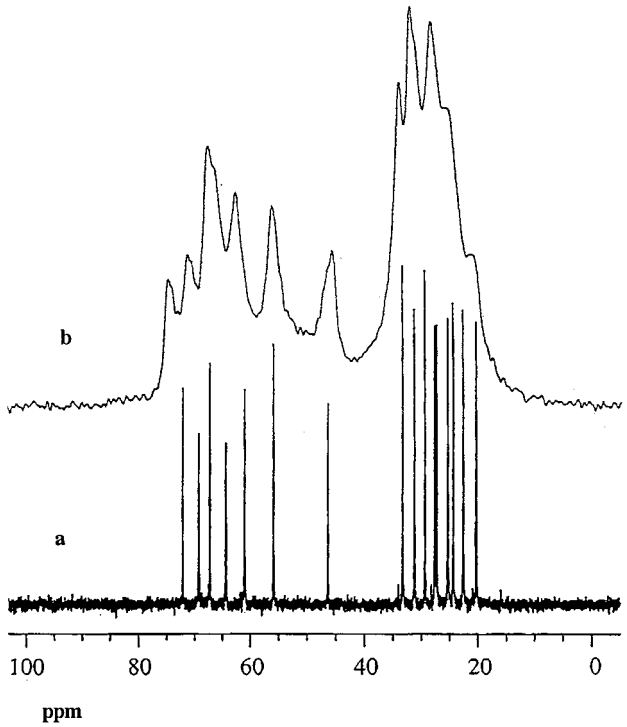

Figure 7. ^{13}C NMR of organic SDA, N(16)-methylspartienium: (a) ^{13}C MAS NMR of as-synthesized pure-silica CIT-5 with SDA occluded in pores and (b) liquid ^{13}C NMR of N(16)-methylspartienium bromide.

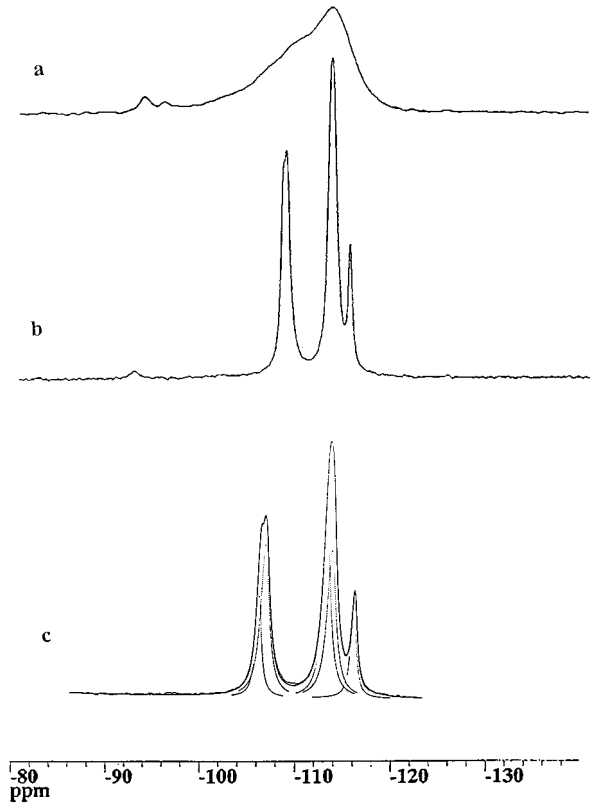

Figure 8. ^{29}Si MAS NMR of (a) as-synthesized pure-silica CIT-5, (b) calcined pure-silica CIT-5, and (c) simulated spectra.

Thermal/Hydrothermal Stability. Thermal and hydrothermal studies were conducted using in situ X-ray diffraction to determine the crystallinity of pure-silica CIT-5 samples as a function of temperature. For investigation of the thermal stability of CIT-5, a dry nitrogen atmosphere was maintained inside the diffraction chamber while the sample temperature was

TABLE 5: Comparison of Adsorption Capacities for CIT-5 and Other Large and Extra-Large-Pore Molecular Sieves

adsorbate	kinetic diam (Å)	adsorption capacity (mL/g) CIT-5	SSZ-24[a]	UTD-1[a]
argon	3.0	0.108	0.109	0.110
n-hexane	4.4	0.092	0.101	0.121
cyclohexane	6.0	0.090	0.114	0.111
2,2-dimethyl butane	6.2	0.093	0.128	0.119
1,3,5-triisopropyl benzene	8.5	0.041	0.011	0.111

[a] Data from ref 16.

TABLE 6: Constraint Index Conversion Data (C6 cracking) for CIT-5 (SAR = 200) at 427 °C

	convn after 10 min on-stream	convn after 430 min on-stream
feed conversion	38%	19.7%
3-methylpentane	52%	27%
n-hexane	24.3%	12.5%
constraint index	0.38	0.42
product distribution		
C6 isomerization[a]	10.1%	12.9%
C5 minus cracking[b]	84.1%	83.3%
aromatics[c]	3.2%	1.1%
dehydrogenation[d]	1.4%	1.3%

[a] C6 products other than hexane and 3-methylpentane. [b] C5 and lower hydrocarbons from cracking (paraffins and olefins). [c] For example, benzene, toluene, etc. [d] C6 olefins.

increased from room temperature to 973 K in 100 K increments as previously described. A water/nitrogen atmosphere was maintained in the chamber during the hydrothermal stability studies.

The pure-silica CIT-5 samples are found to be both thermally and hydrothermally stable to over 923 K. These results are consistent with the thermal/hydrothermal stabilities of other large- and extra-large-pore high-silica zeolites and, together with the previously reported stability studies of UTD-1,[16] indicate that extra-large-pore materials can have the thermal and hydrothermal stability required for industrial application.

Catalytic Studies. Table 6 summarizes the results from the cracking of C6 isomers (*n*-hexane and 3-methylpentane). The values for the constraint index (CI = log(fraction *n*-hexane remaining)/log(fraction 3-methylpentane remaining))[30] calculated for the C6 cracking over CIT-5 indicate that the cracking activity is consistent with the extra-large pores of CIT-5 (CI < 1, indicating no shape-selective preference for the linear hydrocarbon). Other large-pore zeolites such as SSZ-24 (CI = 0.35, 73% conversion), SSZ-31 (CI = 1.20, 50% conversion), USY (CI = 0.25, 50% conversion), and UTD-1 (CI = 0.35, 78% conversion) show similar results. ZSM-5 (CI = 5.0, 70% conversion) and ZSM-12 (CI = 1.8, 20% conversion), which both have smaller pores, show some shape-selectivity (CI > 1). As can be observed from the data shown in Table 6, the catalyst does steadily deactivate. However, during the decline in activity, the ratios reported are unaffected by the gradual coking. These results indicate that there exist acid sites within the material that are strong enough to crack alkanes and, additionally, that there is no selective narrowing of the pores or change in the reaction site as has been seen for zeolites beta and MCM-22.[31]

The acidic forms of Al-substituted (sample A) and Ga-substituted (sample B) CIT-5 were used in *m*-xylene reactions. Both samples showed similar product selectivities and activities. The results described below are from sample B.

m-Xylene isomerization selectivity of CIT-5 and other zeolites is shown Table 7. The large pore diameter of CIT-5 is evident by the low ratio of *p*- to *o*-xylene isomers (*p*/*o* ratio). The *p*/*o* ratio from CIT-5 is similar to the ratio of products from reaction over one-dimensional large- and extra-large-pore zeolites SSZ-31, SSZ-24, and UTD-1. Zeolites with smaller pore sizes, such as ZSM-12, show a higher *p*/*o* ratio, indicating some shape-selectivity. As with C6 cracking, CIT-5 steadily deactivates when accomplishing the *m*-xylene conversions, but the *p*/*o* ratio does not change with time on-stream. In contrast, the *p*/*o* ratio from reaction over UTD-1 steadily increases with time on-stream, indicative of a selective narrowing of the pores by coking.

TABLE 7: *m*-Xylene Isomerization for CIT-5 (Selectivities Extrapolated to Zero Time On-Stream)

molecular sieve	pore size (nm)[a]	initial *p*-xylene/*o*-xylene selectivity
CIT-5	0.73	0.60
SSZ-24	0.73	0.77
UTD-1	0.875	0.66
SSZ-31	0.715	0.75
ZSM-12	0.57	1.27
USY	0.74 + mesopores	1.12
ZSM-5	0.545	2.68

[a] Pore diameter of the largest pore. If pore is not circular, the average is used.

TABLE 8: Trimethylbenzene Selectivities for CIT-5 and Other Zeolites

zeolite	trimethylbenzene isomer (%) 1,2,3	1,2,4	1,3,5
CIT-5	8	83.5	8.5
ZSM-12	0	100	0
UTD-1	7	71	22
USY	6.5	66	27.5
SSZ-24	9	83.5	7.5
SSZ-31	7	76	17
ZSM-5	0	100	0
equilib at 350 °C	8	68	24

In addition to isomerization, *m*-xylene can disproportionate into trimethylbenzenes (TMBs) and toluene. The distribution of trimethylbenzene isomers reflects important structural features such as pore size and shape.[32] Larger-pore zeolites tend to have a trimethylbenzene distribution that approaches equilibrium. However, structures with smaller-sized void spaces tend to suppress the formation of the bulky 1,2,3 and 1,3,5 isomers. The data in Table 8 illustrate the TMB selectivity of CIT-5 and several other zeolites. Reaction of *m*-xylene over CIT-5 produces trimethylbenzenes with a low abundance of the bulky 1,3,5 isomer relative to equilibrium or reaction over the larger-pore UTD-1. Similar results are observed for the reaction over SSZ-24, as might be expected.

For the experimental modeling of hydrocracking reactions, the *n*-hexadecane feed was carried out at 96% conversion (for comparison to other catalysts tested previously). Santilli and co-workers[33] described an *inverse* shape-selective phenomenon in which isomerized cracked products are preferred over straight-chain hydrocarbons as the pore wall dimensions more closely match the kinetic diameters of the potential products. This behavior was shown to be particularly effective in the promotion of dimethylbutane products from *n*-hexadecane hydrocracking via the SSZ-24 catalyst with a pore diameter near 7.3 Å.[33] Upon comparison of the ratio of the formed dimethylbutanes to *n*-hexane versus pore diameter, a bell-shaped curve is observed where the ratio is low for pore systems below 6 Å (the dimethylbutanes would be hindered from diffusing out of the constricted pores); higher values are achieved for 12-ring

TABLE 9: Hydrocracking of *n*-Hexadecane. Comparison of Dimethylbutanes to *n*-Hexane Product Ratios with Pore Diameters

molecular sieve	dimensionality	diameter (Å)	dimethylbutane/ *n*-hexane
ZSM-12	1	6.0	0.08
SSZ-31	1	8.8 × 5.5	0.50
SSZ-24	1	7.3	0.80
CIT-5	1	7.3[b]	0.33
UTD-1	1	10.0 × 7.7	0.20
LTL	1	10[a]	0.20
FAU	3	13[a]	0.15

[a] Multidimensional channel system. [b] Small side pockets within pores give maximum free pore diameter of 10.7 Å.

zeolites, and then for larger pores the effect of the inverse shape-selectivity is lost and the values drop again for this ratio. This ratio for several zeolites and CIT-5 is presented in Table 9 along with the nominal pore-size data. A particularly interesting case is SSZ-31[34] which has an elliptical, one-dimensional pore that reaches 8.8 Å in diameter across the major axis of the ellipse but is limited to 5.5 Å in diameter across the minor axis. In this case, the smaller cross section determines the product distribution. SAPO-11, another molecular sieve with elliptical pores and a diameter across the major axis greater than 6 Å, also shows this restrictive behavior. Although the pore aperature is 7.3 Å, CIT-5 does not give a ratio near the maximum of the bell-shaped curve, as SSZ-24 does. Instead, the hydrocracking over CIT-5 yields a lower ratio, which can be attributed to small side pockets that give a maximum free pore diameter of 10.7 Å. The reaction data when taken in total show that CIT-5 provides for unique reaction behavior when compared to other zeolites. This is not unexpected from the fact that it contains a unique pore system.

Conclusions

The structure of CIT-5, a new high-silica molecular sieve, has been determined, and the material is shown to contain extra-large pores circumscribed by 14 T-atoms. Rietveld refinement of the synchrotron X-ray powder data gives the symmetry and space group assignment for the structure of $Pmn2_1$ (no. 31) with refined unit cell parameters of $a = 13.6738(8)$ Å, $b = 5.0216(3)$ Å, and $c = 25.4883(7)$ Å ($V = 1750.1$ Å^3). All Si−O−Si and O−Si−O bond angles and Si−O bond distances calculated from the final atomic coordinates are within reasonable ranges for silicate materials. TEM/ED indicates that the one-dimensional pore material does not contain faulting defects and that the pores run along the long axis of the crystals. Both the adsorption (1,3,5-triisopropylbenzene uptake) and the catalytic results (*p*/*o* ratio from *m*-xylene isomerization and the dimethylbutane/*n*-hexane product ratio from the hydrocracking of *n*-hexadecane) support the structure assignment. CIT-5 is synthesized hydrothermally in the presence of the organic, N(16)-methylsparteinium, and lithium cations. ^{13}C MAS NMR indicates the organic is intact in the pores of the as-synthesized material and has not degraded under synthesis conditions. Stability studies reveal that CIT-5 retains its pore structure under both high thermal and hydrothermal conditions. CIT-5 together with UTD-1 are the only extra-large-pore, high-silica molecular sieves that have high thermal/hydrothermal stability.

Acknowledgment. We gratefully acknowledge Dr. John Higgins of Air Products and Chemicals Inc. and Dr. D. E. Cox for their assistance in collecting the synchrotron powder XRD data. The data were collected at the X7A beamline at the National Synchrotron Light Source at Brookhaven National Laboratory (Upton, NY), which is supported by the Department of Energy, Division of Material Science and Division of Chemical Sciences. Dr. Chuck Kibby of Chevron is thanked for the collection of argon isotherms, Dr. Ronald C. Medrud of Chevron is thanked for synchrotron powder XRD data collection, and Drs. Tom Harris and Bowman Lee also of Chevron are thanked for the experimental hydrocracking and cracking data. M.T. and M.L. acknowledge support from the David and Lucile Packard Foundation. P.W. thanks Air Products and Chemicals for financial support. Additional financial support for this work was provided by Chevron.

References and Notes

(1) Davis, M. E. *Chem. Eur. J.* **1997**, *3*, 1745−1750.
(2) Davis, M. E. *Chem. Ind. (London)* **1992**, *4*, 137.
(3) Estermann, M.; McCusker, L. B.; Baerlocher, Ch.; Merrouche, A.; Kessler, H. *Nature* **1991**, *352*, 320−323.
(4) Davis, M. E. *Nature* **1991,** *352*, 281.
(5) Davis, M. E. *Nature* **1989**, *337*, 117.
(6) Barrer, R. M.; Villiger, H. *Z. Kristallografiga* **1963**, *128*, 352.
(7) Smith, J. V.; Dytrych, W. J. *Nature* **1984**, *309*, 607.
(8) Brunner, G. O.; Meier, W. M. *Nature* **1989**, *337*, 147.
(9) Davis, M. E.; Saldarriaga, C.; Montes, C.; Garces, J.; Crowder, C. *Nature* **1988**, *331*, 698.
(10) Jones, R. H.; Thomas, J. M.; Chen, J. S.; Xu, R. R.; Hou, Q. S.; Li, S. G.; Ma, Z. *J. Solid State Chem.* **1993**, *102*, 202−208.
(11) Loiseau, T.; Ferrey, G. *J. Solid State Chem.* **1994**, *111*, 403−415.
(12) Loiseau, T.; Ferrey, G. *J. Mater. Chem.* **1996**, *6*, 1073−1074.
(13) Kahn, M. I.; Meyer, L. M.; Haushalter, R. C. *Chem. Mater.* **1996**, *8*, 43−53.
(14) Schindler, M.; Joswig, W.; Bauer, W. H. *Z. Anorg. Allg. Chem.* **1997**, *623*, 45−54.
(15) Freyhardt, C. C.; Tsapatsis, M.; Lobo, R. F.; Balkus, K. J.; Davis, M. E. *Nature* **1996**, *381*, 295.
(16) Lobo, R. F.; Tsapatsis, M.; Freyhardt, C. C.; Khodabandeh, S.; Wagner, P.; Chen, C. Y.; Balkus K. J.; Zones, S.; Davis, M. E. *J. Am. Chem. Soc.* **1997**, *119*, 8474−8484.
(17) Wagner, P.; Yoshikawa, M.; Lovallo, M.; Tsuji, K.; Tsapatsis, M.; Davis, M. E. *Chem. Commun.* **1997**, 2179−2180.
(18) Lobo, R. F.; Davis, M. E. *Microporous Mater.* **1994**, *3*, 61.
(19) Zones, S. I.; Nakagawa, Y. U.S. Patent 5,225,179; 1993.
(20) Bialek, R.; Meier, W. M.; Davis. M. E.; Annen, M. J. *Zeolites* **1991**, *11*, 438−442.
(21) Richardson, J. W.; Smith, J. V.; Han, S. X. *J. Chem. Soc., Faraday Trans.* **1990**, *86*, 2341.
(22) Meier, W. M.; Olson, D. H.; Baerlocher, Ch. *Atlas of Zeolite Structure Types*, 4th ed.; Elsevier: London, 1996.
(23) Werner, P. E.; Erikson, L.; Westdahl, M. *J. Appl. Crystallogr.* **1985**, *18*, 367.
(24) Larson A. C.; Von Dreele, R. B. *Los Alamos Laboratory Report*, 1987, No. LA-UR-86-748.
(25) Baerlocher, Ch.; Hepp, A.; Meier, W. M. *DLS-76: A Fortran Program for the Simulation of Crystal Structures by Geometric Refinement*, Institute fur Kristallographie, ETH: Zurich, Switzerland, 1977.
(26) *CERIUS Molecular Simulations*, version 3.2; Cambridge, U.K., 1993.
(27) Thompson, P.; Cox, D. E.; Hastings. J. B. *J. Appl. Crystallogr.* **1987**, *15*, 615−620.
(28) Lewis, J.; Freyhardt, C. F.; Davis, M. E. *J. Phys. Chem.* **1996**, *100*, 5045−5049.
(29) Englehardt, G.; Michel, D. *High-resolution solid-state NMR of silicates and zeolites*; Wiley: New York, 1987.
(30) van Bekkum, H.; Flanigen, E. M.; Jansen, J. C. *Introduction to Zeolite Science and Practice*; Elsevier: Amsterdam, 1991.
(31) Yuen, L. T.; Geilfuss, J.; Zones, S. I. *Microporous Mater.* **1997**, *12*, 229.
(32) Martens, J. A.; Perez-Pariente, J.; Sastre, E.; Corma, A.; Jacobs, P. A. *Appl. Catal. A* **1988**, *45*, 85−101.
(33) Santilli, D. S.; Harris, T. V.; Zones, S. I. *Microporous Mater.* **1993**, *1*, 329−341.
(34) Lobo, R. F.; Tsapatsis, M.; Freyhardt, C. F.; Chan, I. Y.; Chen, C. Y.; Zones, S. I.; Davis, M. E. *J. Am. Chem. Soc.* **1997**, *119*, 3732−3744.